I-V characteristics and differential conductance fluctuations of Au nanowires

H. Mehrez, Alex Wlasenko, Brian Larade, Jeremy Taylor, Peter Grütter, and Hong Guo
Center for the Physics of Materials and Department of Physics, McGill University, Montreal, PQ, Canada H3A 2T8.

Electronic transport properties of Au nano-structure are investigated using both experimental and theoretical analysis. Experimentally, stable Au nanowires were created using mechanically controllable break junction in air, and simultaneous current-voltage (I-V) and differential conductance $\delta I/\delta V$ data were measured. The atomic device scale structures are mechanically very stable up to bias voltage $V_b \sim 0.6V$ and have a life time of a few *minutes*. Facilitated by a shape function data analysis technique which finger-prints electronic properties of the atomic device, our data show clearly differential conductance fluctuations with an amplitude $> 1\%$ at room temperature, and a nonlinear I-V characteristics. To understand the transport features of these atomic scale conductors, we carried out *ab initio* calculations on various Au atomic wires. The theoretical results demonstrate that transport properties of these systems crucially depend on the electronic properties of the scattering region, the leads, and most importantly the interaction of the scattering region with the leads. For ideal, clean Au contacts, the theoretical results indicate a linear I-V behavior for bias voltage $V_b < 0.5V$. When sulfur impurities exist at the contact junction, nonlinear I-V curves emerge due to a tunnelling barrier established in the presence of the S atom. The most striking observation is that even a single S atom can cause a qualitative change of the I-V curve from linear to nonlinear. A quantitatively favorable comparison between experimental data and theoretical results is obtained. We also report other results concerning quantum transport through Au atomic contacts.

I. INTRODUCTION

Electron transport through atomic nano-contacts has been an active research area for a decade both experimentally and theoretically. The scientific interest of these systems is largely driven by their peculiar electronic and transport behavior. The atomic nano-contacts are structures with low atomic coordination number and, as a result, can behave very differently from the bulk counterpart. From a practical point of view, understanding the novel electronic and structural properties of the atomic nano-contacts is an important step towards nano-device fabrication and characterization. The first set of experiments on nano-contacts focused on their zero bias conductance (G) using Scanning Tunnelling Microscopy (STM)[1–17], Mechanically Controllable Break Junction (MCBJ)[18–24], and Relay Contacts (RC)[25,26]. In these experiments a narrow constriction with a few atoms at the cross section is formed. As the electrodes are pulled apart, G is measured and found to change discontinuously forming plateaus with values close to $n \times G_0$; where n is an integer and $G_0 = 2e^2/h \simeq \frac{1}{12.9K\Omega}$ is the conductance quanta. Pioneering experiments[9,10] clearly showed the correlation between conductance jumps and mechanical properties in the nano-contacts. These results confirmed earlier predictions[27] that the conductance variations are due to abrupt changes of nano-structure cross section as a function of wire elongation. Extensive theoretical investigations on nano-structures have been published recently to analyze these systems. One major theory focus is to calculate the zero bias conductance through a ballistic quantum point contact. These calculations start by assuming various contact[28–39] geometry, or by using more realistic atomic positions derived from molecular dynamics simulations. The potential of the constriction and/or interaction Hamiltonian is then constructed[40–51] from which the zero bias transport coefficients are evaluated. While different levels of approximations were employed in these theoretical analysis, density functional theory based *ab initio* analysis have also been reported[33,36,52] which provide self-consistent calculations of atomic nano-contacts.

While zero bias transport coefficients have received a great deal of attention, one must go beyond this limit to understand the full nonlinear current-voltage (I-V) characteristics of the nano-contacts, as this information is essential for the understanding of real device operation. For example, due to the small cross section of these systems, they are exposed to substantial current density $\sim 10^8 A/cm^2$ which may result in atomic rearrangement. It is also expected that electron-electron (e-e) interaction is enhanced due to the strong lateral confinement possibly leading to Luttinger liquid behavior for the *quasi one dimensional* atomic wires. Separating these different effects is experimentally challenging due to the many variables which can affect the results. This is probably the origin of the existing controversy in explaining the experimentally observed non-linear I-V curves of the atomic scale wires[53–56]. From a theoretical point of view, this is also a challenging problem: so far only two computationally accurate techniques exist which can treat systems with *open boundaries* out of equilibrium due to external bias[33,57,58]. In the approach of Taylor *et. al.*[57,58], realistic atomic leads can be treated and the problem is solved self consistently within LDA. Therefore, the leads, the device (scattering region) and their couplings are incorporated without any preconditioned parameters.

To further shed light on the physics of quantum transport at molecular scale, we report in this paper our investigation on transport properties of Au nanostructures both experimentally and theoretically. Experimentally, we created stable Au nanowires using the mechanically controllable break junction technique in air, and we si-

multaneously measure the I-V curve and the differential conductance $\delta I/\delta V$. We found that our atomic scale Au nano-contacts are mechanically very stable up to bias voltage $V_b \sim 0.6V$ and have a life time of a few minutes which is adequate for our measurements. As we are interested in features due to electronic degrees of freedom of the nano-contacts, careful data analysis is needed because transport data can be affected by many factors. By defining the *shape function*, $S = \frac{\delta I}{\delta V}\frac{V}{I}$, which fingerprints electronic properties of the atomic device, our data clearly shows differential conductance fluctuations with an amplitude $> 1\%$ at room temperature, and a nonlinear I-V characteristics. To understand these transport features, we carried out *ab initio* calculations on various Au atomic wires bonded with atomic Au electrodes using the first principles technique of Ref. 57,58. Our calculations show that pure and perfect Au nanocontacts do not give the nonlinear I-V curves as measured in the experiments. However when Sulfur impurities are present near the wire-electrode contact region, the nonlinear I-V curves emerge due to the tunnelling barrier provided by the impurity atoms. The most striking observation is that even a single S atom can cause a qualitative change of the I-V curve from linear to nonlinear. A quantitatively favorable comparison between experimental data and theory results is then obtained. Our combined theory-experiment investigation allows us to conclude that transport through Au atomic wires is strongly affected by the properties of the wire-electrode contacts.

The rest of the paper is organized as follows. In the next section, experimental measurement and results are presented. Section III presents the theoretical results while Section IV discusses the transmission coefficients in more detail. We also discuss and compare previous works with ours in section V, followed by a conclusion.

II. EXPERIMENTAL RESULTS

Atomic scale gold contacts were formed with a mechanically controllable break junction in air at room temperature. Once suitably stable atomic junctions were formed, a slowly varying bias voltage was applied (typically a $0.1Hz$ triangle wave, $2V_{p-p}$) along with a small modulation voltage (typically $40kHz$, $4mV_{rms}$) across the contact and a load resistor of $3K\Omega$. Current (I) and differential conductance ($\delta I/\delta V$) were measured with an I-V preamplifier and a lock-in amplifier. The experimental set up is shown in Fig.1-a. A typical measurement through a stable Au nano-contact is presented in Fig.1-b. We show our data for the differential conductance and the DC conductance ($G = I/V$). In the inset of Fig.1-b, we also display a typical I-V measurement. This data was taken over the course of a 5 seconds voltage sweep from positive (dark lines) to negative (grey lines) bias voltage (V). Both polarities share a common overall shape, but seem to vary significantly in the details of their conductance behavior. However, for each polarity, one notices that there seem to be similar details present in the DC and differential conductance.

An important issue in order to understand these results is the separation of effects due to atomic rearrangement in the nano structure from electronic properties. We address this problem by writing, very generally:

$$I(X,V) \equiv g(X)f(X,V) \tag{1}$$

where the variable X symbolizes the effects of atomic structure, but no explicit knowledge of X is required. We define $g(X)$ as the unbiased conductance and $f(X,V)$ is the normalized functional form of the voltage dependence of the current. Therefore, in the zero bias limit $V \to 0$, $f(X,V) = V$. We further define a new quantity called the "shape function" (S),

$$S \equiv \frac{\delta I}{\delta V}\frac{V}{I} \quad . \tag{2}$$

Fig.2-a plots S corresponding to the data of Fig.1-b, for both positive and negative bias voltages. The similarity between the curves of the shape functions for both polarities, including fine details, is in striking contrast to the easily distinguishable conductance plots of Fig.1-b. By its definition (Eq. 2), S depends only on f, the functional form of $I(X,V)$, and is independent from the zero-bias conductance $g(X)$. This fact and the usefulness of the shape function S can be seen by considering the following "Gedanken experiment". Let's assume that we measured I and $\delta I/\delta V$ through a variable, ohmic potentiometer as a function of the applied voltage. Suppose there were drastic changes in the temperature during the measurement, and some troublemaker stochastically turned the knob of the variable potentiometer without telling anyone. Glancing at the measurements of $I(X,V)$ and $\delta I/\delta V$ alone, one might wrongfully conclude that the potentiometer was exhibiting a nonlinear behavior. However, a plot of S would show that $S(V) = 1$ (from Eq.2), which would allow us to deduce that the I-V curve was actually linear and thus in fact ohmic. One would also conclude that the origin of the apparently nonlinear behavior was due to a change in the unbiased conductance $g(X)$, rather than due to a true nonlinearity in voltage.

Returning to the experimental results shown in Fig.2-a, we note the overlap of the two curves of S for positive and negative bias voltages; this points to a similar functional form for both bias polarities. Because of this, we deduce that for this case $f(X,V)$, at most, depends very weakly on X (especially at bias voltage $V_b < 0.47V$). We can therefore write $f(X,V) \simeq f_0(V) \propto e^{\int \frac{S}{V} dV}$, and the unbiased conductance $g(X) = \frac{I(X,V)}{f_0(V)}$. Hence, as an experimental voltage sweep typically takes 5 seconds, time dependent atomic rearrangements (changes in X) manifest themselves as stochastic variations of $g(X)$. Other details of this data analysis technique and further discussion on the shape function are not within the scope of

this paper and can be found elsewhere[59].

The normalized functional form of the voltage dependence of $f_0(V)$ for the measured data is shown in Fig.2-b. We note that the curves for both polarities appear on the top of each other and they are indistinguishable. However, as expected, the "trouble maker" in our "Gedanken" experiment shows up as fluctuations in $g(X)$ shown in Fig.2-c, indicated by the fluctuations and by the fact that positive and negative bias give different traces of $g(X)$. Note that during the course of our bias sweep from initial bias voltage to some bias value $V = V_1$, the atomic structure has been fluctuating and changed from what we started with to something unknown. But if we could freeze the structure at that moment and re-measure the $I - V$ curve for the fixed structure, $g(X)$ would be its zero bias conductance. In other words, Fig. 2-c shows a parametric plot of what the conductance $g(X)$ would be at zero bias at the point in time when this voltage was measured experimentally; hence $g(X)$ could also be viewed as a function of time in this figure. Our analysis show that the fluctuations of $g(X)$ which are less than 5% peak-peak, are attributed to changes in the atomic configuration of the junction. We have also found that $g(X)$ exhibits no time correlation and its Fourier Transform has a $1/\mathbf{f}$ frequency behavior.

In Fig.2-d we plot the *normalized* differential conductance, $\delta f/\delta V$. Examining the curves in Fig.2-d, we can see the same subtle fluctuations in $\delta f/\delta V$ as those found in S (Fig.2-a). Both plots show broad and fine details that are uncorrelated to the fluctuations of the unbiased conductance $g(X)$ (Fig.2-c). These plots reveal that it is the fluctuations of the $g(X)$ which dominate the fluctuation features in the measured $I(X, V)$ and $\delta I/\delta V$.

Over different voltage ranges $(0.2 - 0.35V, 0.1 - 0.35V, 0.1 - 0.5V)$, $\delta f/\delta V$ has a high correlation[60] of 0.99 between both polarities. Over these same ranges, $g(X)$ had a weak correlation $(-0.5, 0.25, -0.2,$ respectively) between both polarities which changed drastically depending on the selected voltage range. We have also calculated the correlations by shifting the voltage of *one* polarity with respect to the other by $\pm 10mV$ (the scale of the fine details) in increments of $1mV$. Over all three ranges, the correlation for $\delta f/\delta V$ had a local maximum for $0V$ shift. No correlation extrema were found in the case of $g(X)$. This quantifies how similar the details in both polarities of $\delta f/\delta V$ are to each other, in contrast to the more easily distinguishable curves for $g(X)$. We thus conclude that the "wiggles" observed in $\frac{\delta f}{\delta V}$ are electronic in nature and they are not variations in $g(X)$.

The "wiggles" (magnified in the inset of figure 2-d) of $\delta f/\delta V$ may actually be much more pronounced than indicated in these plots. They are smeared out by unavoidable experimental constraints. Since we must add a modulation signal to make our lock-in measurement of $\delta I/\delta V$, we end up averaging over a range of V. This leads to broadening and decrease in amplitude of these fine details[59,61]. This unavoidable averaging artifact keeps us from making a more precise measurement of the shape, amplitude and voltage characteristics of this fine structure, but the true features should be sharper and more pronounced than they are measured to be. From our data, we observe "wiggles" on the voltage scale $< 10mV$ and with amplitude $\sim 1\%$ of the signal. The width of these fluctuations is comparable to the modulation voltage, $4mV_{rms} \sim 10mV_{p-p}$; hence, it is possible to have features on a voltage scale $< 10mV$ with amplitude which is orders of magnitude larger than these 1% fluctuations.

If one were to merely examine our $I(V)$ measurements, similar results have been observed in air and at low temperatures with RC[25,55] and STM configurations[56,62]. The fine details exposed by the analysis presented above have not been discussed in the literature as they tend to be hidden by the fluctuations in the unbiased conductance $g(X)$ (see Fig.2-c). The data presented here represents the behavior of one junction. However, we emphasize that the general features presented in Fig.2 are experimentally found to be independent from the zero bias conductance $g(V = 0)$ for values between 1 - 10 G_o. The fine details of $\delta f/\delta V$ are reproducible for a given stable junction, but the specific details change for different junctions. Although there seems to be a voltage scale associated with these details ($< 10mV$), Fourier analysis does not indicate any strong periodicity. It should be noted that we have imposed a selection rule on the junction type by studying device configurations that are stable on the time scale of minutes. We have also observed junctions that exhibit linear behavior ($S = 1$) as have others[25,55,56]. These junctions however are not stable over this long time scale. In comparison to their nonlinear counterparts, linear junctions have smaller fluctuations in $g(X)$.

In the following we will discuss the physical origin of the observed $I(V)$ characteristics. In this aspect we will investigate the electronic effects rather than the structural parameters which will be assumed static. This will allow us to gain valuable insight into the voltage dependent conduction properties of nanoscale electrical contacts. We will thus compare our modeling to the normalized functional form of the current, $f_0(V)$, shown in Fig.2-b, rather than the original I-V curve presented in the inset of Fig.1-b. We will also explain the origin of the fluctuations in the normalized differential conductance shown in Fig.2-d as well as the effects of temperature and modulation signal on their amplitude.

III. AB INITIO ANALYSIS OF THE I-V CHARACTERISTICS

To provide a theoretical understanding of the experimental data presented above, we have calculated the I-V characteristics of Au nano-contacts self consistently by combining the density functional theory and the Keldysh

nonequilibrium Green's functions. The method is based on the newly developed *ab initio* approach to treat open electronic systems under finite bias. For technical details of this method we refer interested readers to the original papers[57,58]. Very briefly, our analysis uses an s, p, d real space LCAO basis set[57,58,63] and the atomic cores are defined by the standard nonlocal norm conserving pseudopotential.[64] The density matrix of the device is constructed via Keldysh nonequilibrium Green's functions, and the external bias V_b provides the electrostatic boundary conditions for the Hartree potential which is solved in a three dimensional real space grid. Once the density matrix is obtained, the Kohn-Sham effective potential $V_{eff}(\mathbf{r}; V_b)$, which includes contributions from Hartree, exchange, correlation and the atomic core, is calculated. This process is iterated until numerical convergence of the self-consistent density matrix is achieved. In this way, we obtain the bias dependent self-consistent effective potential $V_{eff}(\mathbf{r}; V_b)$, from which we calculate[57,58] the transmission coefficient $T(E, V_b) \equiv T(E, [V_{eff}(\mathbf{r}, V_b)])$, where E is the scattering electron energy and T is a function of bias V_b through its functional dependence on $V_{eff}(\mathbf{r}; V_b)$.

In our analysis, the scattering states are defined for energy ranges between the left and right chemical potentials μ_L and μ_R, respectively. To solve for these states, at a given energy E, we solve an inverse energy band structure problem[58]. We then group all states as left and right propagating states depending on their group velocity. For a scattering state coming from the left lead, $\Psi^{K_n^L}$ should start as a right propagating state $\Phi_L^{K_n^L}$ and it gets reflected back as a left propagating state $\phi_L^{K_m^L}$ with reflection coefficient $r^{K_m^L, K_n^L}$ in the left lead, and transmitted into the right lead as a right propagating state $\phi_R^{K_m^R}$ with transmission coefficient $t_R^{K_m^R, K_n^L}$. In the numerics, the scattering states are represented as a linear combination of atomic orbitals inside the device region. This allows us to write, for example, a left scattering state as:

$$\Psi^{K_n^L} = \begin{cases} \Phi_L^{k_n^L} + \phi_L^{K_m^L} r^{K_m^L, K_n^L} & \text{inside left lead} \\ \psi_d^{K_n^L} & \text{inside device} \\ \phi_R^{K_m^R} t^{K_m^R, K_n^L} & \text{inside right lead} \end{cases}$$

A scattering state in the right lead can be written in a similar fashion. For a symmetric two probe device, the total transmission from the left lead is identical to the one from the right lead[65]. To calculate the total current inside the device at a given bias voltage V_b applied to the right lead, we use:

$$I(V_b) = \frac{2e}{h} \int_{-\infty}^{+\infty} dE\, T(E, V_b)[f_L(E, \mu_L = \mu_0) - f_R(E, \mu_R = \mu_0 + eV_b)] \quad (3)$$

where $f_{L(R)}$ is the Fermi function on the left (right) lead evaluated at temperature $T = 0K$ unless otherwise stated. In addition to predicting the overall transport properties of a device, our formalism enables us to study transmission through *each* incoming Bloch state of the leads separately, therefore allowing us to separate effects due to the leads and due to the scattering region. We have used this formalism to calculate I-V characteristics of structurally different Au nano-contacts and compared them with the experimental results described above.

A. Perfect Au nano-contacts

In a first attempt to model our experiments, we calculated the I-V characteristics of *four* Au atoms (="molecule") in contact with Au(100) leads. The structure of the atomic device is illustrated in Fig.3-a. The scattering region is bonded by two semi-infinite Au leads which extend to electron reservoirs at $\pm\infty$ where bias voltage is applied and current is collected. The device scattering region, indicated by D, is described by *three* Au layers from the left lead, the *four* Au atoms in a chain, and *two* layers of Au from the right lead. We have also increased the *two* Au layers on the right side of the chain to *four* to ensure that convergence is reached with respect to the screening length. We note that long and thin gold necks have directly been observed experimentally[50].In this structure, the registry of the atomic chain with respect to lead surface layer can be different. The most common structures, which we analyze in this work are: the hollow site, where the atomic chain faces the vacant position in the lead layer as shown in the upper left inset of Fig.3-B; and the top site, where the atomic chain and an atom from lead surface layer face each other as illustrated in the upper right inset of this figure.

Our calculations show that in all cases charge transfer between the Au chain and the leads is not important, being only $\sim 0.07-0.1$ electrons per atom to the Au chain at different bias voltages. This corresponds to less than 1% difference in electron population per atom and therefore does not play any significant role in the I-V characteristics of Au contacts. This is in contrast to a binary atomic system such as carbon chains between Al(100) leads[66]. In addition, solving for the energy eigenvalues of the *four* atom chain gives a HOMO-LUMO gap of $0.68eV$, indicating that the molecule eigenstates should only have a secondary effect on the transport properties. Therefore, the major effect on the I-V characteristics is due to the character of Bloch states in the leads and their couplings to the molecule at the chain-lead interface.

In Fig.3-A, we show the results for a system with atoms in the hollow site. At small bias V_b, we note that current is a linear function of V_b with a slope $G \simeq 0.94 G_o$. The linear function suggests that $T(E, V) = T_0$ with a weak voltage dependence. In this regard, our self-consistent calculation gives a result apparently similar to previous theoretical work[28–51] in the low bias regime. However, we will show later, by addressing the origin of this "perfect

linearity", that the physical picture of a bias-independent transmission coefficient is not valid even for such a simple chain. We also note that the linear I-V characteristics observed in these systems do not agree with our experimental data.

A major feature of Fig.3-A is the huge plateau at $V_b = 0.5V - 0.9V$, as well as the fine structures (or sometimes negative differential resistance) observed for larger voltages. In the lower inset of Fig.3-B, we show the band structure of the Au(100) lead along the $z-$direction (transport direction). Even-though at a given energy E there are many Bloch states which are potential candidates for transporting current, our investigation found that for $E < 0.5eV$ there is only *one state* that is actually conducting (presented by a continuous line in the inset). Once this state is terminated at $E \approx 0.5eV$, the current is saturated resulting in a large plateau until new conducting states emerge at higher bias voltages. For $E > 0.9V$, transport properties are more complex since more states contribute to transmission. Under these circumstances, band crossing occurs more frequently and $T(E, V_b)$ changes over small ranges of bias leading to the small structures seen in the I-V characteristics of perfect Au contacts. In fact these variations in $T(E, V_b)$ are the origin of the fluctuations in the normalized differential conductance shown in Fig.2-d. They thus need to be attributed to the effects of the leads' band structure. In the lower inset of Fig.3-A, we plot the theoretical $\delta I/\delta V$. The magnitude of these conductance fluctuations is of the order of 60% at zero temperature which is much larger than the experimental finding. However, these fluctuations are reduced to 15% if the current is calculated using Eq.3 at a temperature $T = 300K$ (the temperature of our experiments). In addition, the fluctuations further decrease to $\sim 1\%$ when current is averaged over the experimental modulation voltage range of $4mV$, completely consistent with our experimental results of Fig.2-d.

The effect of site registry is studied by placing the end-atom of the Au chain at the top site of the leads. In this situation the chain atoms are facing one atom of the leads' surface layers. This analysis is quite important, because it was shown[46,47] that atoms at the junction change registry from hollow to top sites resulting in bundle formation just before the nano structure breaks. The I-V characteristics of these systems (shown in Fig.3-B) are similar to the previous results, therefore no change is observed in the transport properties for the top site registry.

To further investigate the huge and peculiar plateau occurring at $V_b = 0.5V - 0.9V$, we have plotted in Fig.4 the charge density at a given energy E, $\rho(E, x, z) = \int dy \rho(E, x, y, z)$. We see clearly that at zero bias $V_b = 0V$, the device property turns from a perfect conductor at $E = 0eV$ (Fig.4-a) to an insulator at $E = 0.68eV$ (Fig.4-c) due to the termination of the conducting state. Here we interpret the charge concentration as the effective bonding strength, or conductance probability. Applying a bias voltage to the system drives it out of equilibrium, and at $V_b = 0.68V$ and $E = 0.68eV$, the charge in the molecule redistributes, but the bonding is still very weak as shown in Fig.4-d, with some molecular regions having *zero charge* and resulting in the large plateau observed in our $I - V$ curve of Fig.3-A,B. This effectively demonstrates the importance of both the energy and the voltage dependence of the transmission coefficient $T(E, V)$. This point will be discussed in more detail in section V. A further point to notice is the difference of zero bias conductance, $G \simeq 0.8G_0$ for the top-site device and $G \simeq 0.94G_0$ for the hollow-site device. This difference is due to a change in the coupling between the chain end-atoms and the surface of the leads. To ensure the same nearest neighbor separation distance for both cases, we end up with *four* nearest neighbors for the hollow site registry and only *one* nearest neighbor for the top site registry. Under these circumstances, the hollow site has a better coupling to the chain and hence a larger conductance.

A pure and perfect Au nano-contact, as studied in this section, shows rich and interesting transport properties. It also gives a good understanding of the origin of the observed differential conductance fluctuations as due to coupling of the Au-chain to the leads' band structure. However, it has a linear I-V curve at small $V_b < 0.5$V, rather than the experimentally observed nonlinear I-V characteristics. How can a nano-contact produce a nonlinear I-V curve such as that of Fig.(1-b) ? The simplest possibility to observe such a phenomenon is to have a tunnelling barrier at the molecule-lead junction whose effect gradually collapses as a function of an increasing bias voltage. Indeed, recent experimental findings indicate that perfectly linear I-V characteristics were reproducibly found in gold-gold nano-contacts in ultra high vacuum[56], while nonlinear effects emerge when the experiment was performed in the air. This suggests that impurities play an important factor. Therefore, one has to go one step further and investigate the effect of impurity and disorder at the Au junction.

B. Au nano-contacts with S impurity

To simulate the effect of an impurity at the contact, we have replaced one of the Au atoms at the interface layer with a sulphur atom. This is presented in the inset of Fig.5. The choice of sulphur is motivated by the fact that in our experimental labs located in down-town Montréal, sulphur is a non-negligible airborne pollutant (diesel exhausts); sulphur atoms bond actively with Au. We also note that the band-width of sulphur, $\sim 10eV$, is much higher than that of Au ($\sim 1eV$), thus a tunnelling barrier is expected to be provided by the presence of S atoms. In this system, charge transfer to the atomic chain is still small, and thus inadequate in explaining the experimentally observed I-V characteristics. We note that the S atom suffers from an electron deficiency $\sim 4\%$. Also due to the presence of the S atom, the coupling of the Bloch states in the leads to the device scattering region is quite

different as compared to the mono-atomic gold structure. When the S atom is present, our calculations found that all Bloch states are coupled to the scattering region, with the highest transmitting mode still being the one corresponding to the conducting mode of the mono-atomic gold system.

The I-V characteristics of the S doped Au nano-contacts is shown in Fig.5. We note that the I-V curve for voltages up to 0.5V is very similar to the experimental values with nonlinearity onset at *non zero* bias voltage. We also note that the huge current plateau of the pure Au device has now diminished because more states contribute to electronic transport. To compare these results with the experimental measurement, we have used the normalized functional form of the voltage, $f_0(V)$ shown in Fig2-b, and multiplied it by the simulated zero bias conductance ($0.67G_0$). The result is shown as open circles in Fig.5. The qualitative and quantitative agreement between the theoretical and experimental results is rather encouraging. In fact, this is the first time that experimental nonlinear I-V characteristics could be compared so well and so directly with *ab initio* self consistent calculations. It is also a very surprising result because a single S impurity can qualitatively alter transport in these nano-contacts from linear to nonlinear.

The I-V curve in Fig.5 still shows the small features similar to those found in pure and perfect Au contacts (presented in Fig.3). These fine details of the calculated I-V curve would result in differential conductance fluctuations similar to the ones shown in the experimental data of Fig.2-d and the pure Au device of Fig.3-b. However, these fine features as calculated are wider and occur at higher bias voltages than the experimentally observed ones. The former can be attributed to the zero temperature we used in our calculation. The absence of these fine features at smaller voltages is attributed to the small size of the leads used in our theoretical modeling: close to E_F there are just a few states so that abrupt variation of $T(E, V_b)$ at smaller V_b is less probable, resulting in a smoother I-V curve at low V_b.

To understand other possible factors which can affect I-V characteristics of nano-contacts we have studied the effect of a larger number of S impurities, disorder, and their combined effects. The results of these calculations are presented in the following subsection.

C. Contacts with several impurities and disorder

Including more S impurities at the contact enhances the tunnelling barrier and may give rise to a smaller current with a larger nonlinear behavior. The result with replacing two Au atoms at the interface by S atoms is plotted in Fig.6-A. Indeed, as expected the I-V curve for this system shows a larger nonlinear character. The nonlinearity starts at $V_b \sim 0.17eV$. It is actually more nonlinear than that of the experimental data; this is mainly due to the high concentration of S at the interface. Therefore, an experiment which dopes an Au contact with more S impurity should show an enhancement of the I-V nonlinearity. This also gives a possible explanation of why experimentally the nonlinear I-V fitting parameters are not universal[53,54]: they dramatically depend on the contact structure as well as the impurity concentration.

Studying the effect of disorder in nano-contacts is another important problem. To investigate this effect, we have randomized the contact layer in the left lead of a pure Au nano-contact, as shown in the inset of Fig.6-B. The distribution of disorder leads to a smaller distance between the contact layer and the Au chain, resulting in a better coupling. The current through this device is larger than that of the ideal contact and is shown in Fig.6-B. For this device, the slope of the current at zero bias is $G \sim 0.915G_o$, and it slightly increases to $G \sim 0.92G_o$ at $V_b \sim 0.2V$. The I-V curve shows very weak nonlinear characteristics. This suggests that disorder alone may create a tunnelling barrier which is overcome through the application of a bias voltage. However, to observe the effect, there need to be conducting states in the scattering region. For our pure Au device, only *one single state* is conducting and the maximum zero-bias conductance is $G = G_o$. Therefore, at $G \sim 0.915G_o$, the conducting channel is already open to near its maximum at zero bias, hence it cannot be further enhanced in any significant way by applying a bias. The results in Fig.6-B show that disorder is an important factor that allows more Bloch states in the leads to couple with the scattering region and contribute to transport properties. This is clearly seen when we notice that the huge current plateau observed in Fig.3 essentially vanishes in disordered device.

Combining the effect of disorder and S impurity is also crucial. The latter enhances the tunnelling barrier and the former may enhance the coupling of the device to the leads. We have used the disordered structure studied in the last paragraph and replaced one of the Au atoms at the contact layer with an S atom, as shown in the insets of Fig.6-C. The zero bias conductance for this device is $G \sim 0.833G_o$. This number is larger than the one with only a tunnelling barrier (ideal contact with S impurity), but is smaller than the one with only a disordered contact (which has better coupling). The final conductance is due to a competition between both effects. The I-V curve for this device is presented in Fig.6-C, it shows very weak nonlinear I-V characteristics: analysis of our data show that the slope reaches $G \sim 0.85G_0$ at $V_b \sim 0.18V$. Therefore, there is still a weak nonlinear behavior, but it is small due to the fast saturation of conducting channel in the device.

From these results we can conclude that the I-V characteristics of an atomic junction is a complex phenomenon in which the leads, eigenstates of the scattering region, as well as impurity and disorder play major roles. In particular, a tunnelling barrier created by impurities can result in nonlinear I-V behavior of the nano-device. However, to be able to observe this effect, conducting channels

in the device need to be present, otherwise transmission saturation is reached at small voltages and a linear I-V characteristics is seen. Formally, it is the transmission coefficient $T(E, V_b)$ that is of crucial importance when analyzing the effect of the eigenstates of the leads and the device, as well as the lead-device coupling.

In the next section we determine the behavior of $T(E, V_b)$ and we will address the following questions: Is the voltage independence of $T(E, V_b)$ an adequate picture? Which $T(E, V_b)$ behavior would result in nonlinear I-V characteristics? Can the major characteristics of $I(V_b)$ be qualitatively estimated from simple arguments or does one always need to perform an extensive ab-initio simulations?

IV. BEHAVIOR OF TRANSMISSION COEFFICIENT $T(E, V_B)$

For all the Au nano-contacts we have investigated theoretically, $T(E, V_b = 0)$ increases as a function of E (for $E < 0.2eV$). A typical behavior is shown in Fig.7-a by a dashed line for an ideal top site, pure and perfect Au device. From this curve, it is clear that there is transmission enhancement as a function of E which should result in a nonlinear I-V curve if $T(E, V_b \neq 0)$ behaves in the same way. In the same graph we have also plotted $T(E, V_b = 0.136V)$. One can observe that the general energy dependence of E is still the same, namely increasing, but there is a global shift of the curve downward. Therefore, an increase in transmission coefficient as a function of E is compensated by its decrease due to increased bias voltage. The total effect on the current is to produce a *linear* I-V curve as shown in Fig.3-B. We also note that this complete compensation between E and V_b is not universal and can be different from one system to another. In fact, even for the same device it can behave differently at different energy ranges. This results in different features in the I-V curves such as plateaus, the "wiggles", etc. as we have discussed previously.

A similar analysis is done on a device with a S impurity. The results are shown in Fig.7-b. For this device it is clear that the effect of E on transmission at $V_b = 0$ is more pronounced. This is evidence that tunnelling is an important factor. In addition to this, we note that applying a bias voltage to the system causes a decrease in the transmission coefficient, but it is not a global decrease. In particular, a bias voltage of $V_b = 0.136$V actually increases transmission at small energies as shown in Fig.7-b. Therefore, the combined effect of E and V_b does not cancel and it gives rise to the nonlinear I-V characteristics as seen in Fig.5. According to this analysis, one can easily predict some aspects of the I-V curves just by studying the transmission coefficient $T(E, V_b)$ at two different bias voltages. Obviously, this helps to predict $I(V_b)$ characteristics with much less computational effort.

In Fig.7-c,d, we do a similar analysis on a device with disorder and one with disorder plus impurity, respectively. Due to the conductance channel saturation effect in the scattering region, the transmission coefficient has a very weak energy dependence (roughly constant). This behavior also emerges in the I-V curve which shows a very weak nonlinear behavior. We conclude that the roughly linear I-V curves of Fig.3-B and Fig.6-B,C are due to very different origins. In the latter case it is due to the channel saturation effect in the scattering region, whereas in the former it is due to a compensation between the effects of increasing energy and bias voltage on $T(E, V_b)$.

V. DISCUSSIONS

We have already shown in the previous sections that transport at the molecular level is a complex phenomenon. To understand these systems, careful experimental work which separates electronic effects from structural relaxations, as well as detailed calculations which include the effects of the molecule, leads and their coupling are required. In this section we discuss and compare our findings with previously published theoretical concepts and experimental results.

Experimental work reported by Costa-Krämer *et. al.*[53,54] have shown clear nonlinear I-V characteristics in Au nano-contacts starting at bias $V_b = 0.1V$, and its origin was attributed to strong e-e interactions. To rule out the impurity effect, the authors[53] have used scanning electron microscopy to analyze contacts of diameter $\sim 300nm$. They also used energy dispersive X-ray analysis and determined a contamination concentration below detection sensitivity. Experimental cleanness checks performed for the large nano-contacts ($\sim 300nm$), however, can not be extrapolated to junctions of few atoms in size due to the exquisite chemical sensitivity as demonstrated by our model. In other experiments[55] with Au relays, it was observed that conductance quantization histogram survived for even larger bias, ($1 \times G_o$ peak persists for $V_b \sim 1.8V$). These data show clearly that in such an experiment nonlinear I-V behavior cannot occur at low bias ($V_b \simeq 0.1V$). We believe that these junctions were formed between atomically clean gold contacts. These experiments were performed by forming and breaking the contacts very quickly ($\sim \mu sc$), thus removing the impurity atoms from the Au junction even if they existed[67]. Recently, elegant experimental work by Hansen *et. al.*[56] found that contaminated Au nanostructure show nonlinear I-V characteristics, whereas experiments done with clean tip-sample in UHV show perfect linearity for $V_b < 0.7V$. The nature of the contamination was not determined.

A fundamental question that is to be addressed in this section, is transport through an impurity the most likely physical picture that can explain the observed nonlinear I-V characteristics. In the following we compare and discuss some of the concepts described in the literature

relevant to this issue.

Free electron models have been used to describe the behavior of nanostructures under external bias[31,39]. In these systems, depending on the potential profile across the device and the external bias voltage drop, various I-V characteristics can be extracted. In passing, we note that these calculations neglected the voltage dependent coupling $T(E, V_b)$ (discussed in Fig.7). This is obviously a major draw back for calculations at the molecular level, as shown by our analysis. However, a voltage drop at the contacts is still a reasonable approximation. In Fig.8, we plot the Hartree potential across the *four* Au-atom chain. It is clearly seen that the potential drops mostly at the interfaces. However, assuming a uniform potential across the constriction is not adequate due to the atomic structure and the small variation of charge transfer as a function of bias voltage.

A self consistent tight binding (TB) model has also been implemented to find the conduction dependence of each eigenchannel in Au nano-contact as a function of bias voltage[68]. In these calculations, the TB parameters are calculated from a bulk system and charge neutrality of each atom of the nano-contact is enforced in order to carry out the self consistent calculations. Although it is not clear if the TB parameters determined from bulk structures are directly transferable to nano-contacts with atoms of low coordination number, especially when put under a bias potential, our *ab initio* results show that charge neutrality is a valid approximation for Au devices without impurities since charge transfer is quite small. In self consistent tight binding models, charge neutrality is accomplished by locally adjusting the chemical potential. For a zero bias calculation and nano-contacts with *three* atoms, Ref. 68 shows that a local potential $\sim 3eV$ needs to be added to the central atom to achieve charge neutrality. This seems to be a large value for Hamiltonian correction. Therefore, we suggest that for pure Au nanostructures, zero bias *ab initio* calculations should be done to extract the TB parameters (rather than from bulk). These can then be used more safely with charge neutrality constraints to deduce I-V characteristics of nano-contacts. Since we have seen only small effects of the bias voltage on the atomic charge transfer for a S doped Au structure in our *ab initio* calculations, we suggest that for this particular structure it is possible to deduce the charge distribution and the TB parameters from zero bias calculations. Using these TB interaction parameters and the zero bias charge at each atom as a constraint, the I-V characteristics of these structures can then be solved self-consistently. The results are less accurate compared to a full *ab initio* calculation, but they should give better results than using the conventional TB parameters derived from bulk systems.

There are other important theoretical calculations going beyond the single particle picture. Since the device constriction is narrow, e-e interaction can be strong and non-Fermi liquid behavior might have to be taken into account. However, it was shown by Maslov and Stone[69] that for these systems the resistance is due to contact and thus the results are independent from the Luttinger liquid behavior in the constriction. Therefore, in these calculations[69] transmission is found to be identical to non-interacting particles. An important, single particle transmission, approximation is incorporated in this model[69]. However, at non-zero temperature or/and bias voltage, a finite number of particles are injected into the nano structure resulting in backscattering effects. These lead to charge accumulation at the interface, creating an extra potential in addition to the original constriction potential. This additional potential is both Hartree (V_H) and exchange-correlation (V_{xc}) in nature, and it is the reason for the so called resistance dipole[70]. Due to this additional potential contribution, it was shown[71] that for 1D systems the transmission coefficient is renormalized. It was further proposed that this charging effect can even close a conducting channel that is 90% transmissive[54]. This channel is gradually opened as V_b is increased for a complete transmission at $V_b \sim 0.35V$, thereby inducing a nonlinear I-V curve. From a theory point of view, the picture of charging induced nonlinear I-V characteristics should overcome two further difficulties: that the renormalized transmission depends on an interaction parameter α which can not yet be determined for atomic wires; and that previous calculations solved a 1D case with no effect of V_b on the transmission $T(E, V_b)$. In the rest of this section, we follow the interesting idea of the charging effect and analyze it in more detail to understand if this effect, which leads to channel closing[53,54] can give rise to nonlinear I-V curves of atomic devices. To start, we follow the work of Yue *et. al.*[71] by assuming a strong interaction and write the renormalized transmission coefficient as[54,71],

$$T^R(E) = \frac{T_0(E/D_0)^{2\alpha}}{R_0 + T_0(E/D_0)^{2\alpha}} \tag{4}$$

where, T_0, R_0 are the transmission and reflection coefficients of the non-interacting model such that $T_0 + R_0 = 1$, and α is a parameter to describe e-e interaction in the constriction. The parameter D_0 is the energy range near E_F which contributes to renormalizing T_0 and is determined[71] by $D_0 = \hbar v_F/W$, where v_F is the Fermi velocity of the system ($10^8 cm/sc$ for Au) and W the width of the nano-constriction[54], $W \sim 10 - 20\mathring{A}$. Therefore, we find that for these devices $D_0 \sim 1.0eV$. From Eq. 4, we compute the current $I(V_b)$ at zero temperature by integrating $T^R(E)$ from zero to eV_b, assuming no bias dependence of $T^R(E)$. The conductance is then deduced by $G = I(V_b)/V_b$. We note that due to the finite length effect of the constriction[54], $L \sim 100\mathring{A}$, the renormalization effect is cut off for bias voltages $V_b < V_s$, where $V_s = 2\pi\hbar v_F/L \sim 0.1D_0$. Within this approach and using the free parameters as specified, we have plotted in Fig.9-a the conductance of a single channel as a function of bias voltage V_b. Qualitatively, the results show that G increases with V_b due to the channel opening. However, quantitatively they do not give a complete

channel opening at the experimental value of $V_b \sim 0.35V$ (as suggested in Ref.54), if the channel is less than 10% transmissive at $V_b = 0$. In fact, we found that a bias of $2V$ is needed to overcome the charging potential barrier, thereby the nonlinearity in I-V curve can only set in at much larger voltages. We also note that since the extra charge due to backscattering is accumulated at the interface which has a larger cross section, we expect that DFT and the local density approximation to V_{xc} should work well. Our self-consistent calculations, with all the charge transfer and re-arrangements accounted for, have already partially included the backscattering effects. Our results show that it is possible to partially close a channel $\sim$ 60%–but not completely. Our experimental data which shows zero bias conductance of $\sim 2.2G_o$, indicate that at least one channel is 20% transmissive and that channels are *only partially closed*, consistent with our theoretical work. Therefore, we can conclude at this point that the physical picture of electron interactions to completely close and open a channel as a function of V_b, while interesting, cannot explain our experimental data.

To further address the importance of backscattering effects[71], especially for our devices with realistic atomic leads, we have investigated the dependence on the interaction parameter α in Eq.(4). Tuning this parameter can dramatically change the renormalized transmission coefficient as a function of V_b as shown in Fig.9-b. Therefore we have a wide range of this parameter for fitting our experimental data. However, if we change the Au nano-contact by only a single sulphur atom, we should not expect a very different e-e interaction parameter α, thereby this would predict an I-V curve not too different from the one without the sulphur. This suggests that strong interaction alone would not predict strong sensitivity of the I-V curve dependence on small amount of impurities, in contradiction to experimental results[55,56]. Transmission renormalization is important in 1D scattering problems where there is no charge in the leads. For realistic atomic leads, the backscattered charge is a small fraction of the original one, and its effect should be well screened. With all these considerations, we believe it is unlikely that the dynamically established charging effect alone is large enough to cause the observed I-V nonlinearity for Au nano-contacts.

VI. CONCLUSION

In this paper, we discuss the electronic transport properties of Au nano-contacts from both experimental and theoretical studies. Our experimental data analysis enables us to separate electronic effects from structural relaxations, allowing a better comparison to theoretical modeling of these nano-devices. Our theoretical work shows that transport properties at the molecular scale need to be analyzed at the systems level: leads, molecule and their interactions have to be studied simultaneously. The self-consistently determined transmission coefficient $T(E, V_b)$ is shown to vary as a function of E and V_b. This gives rise to differential conductance fluctuations of the order of 1% at temperature $300K$ taking into account the experimental averaging process. These fluctuations are attributed mainly to the effects of the lead band structure. Most striking, however, is the fact that a single impurity atom at the contact region can alter I-V curves qualitatively in these devices: pure and perfect Au nano-contacts do not give the observed nonlinearity, while a sulfur doped device does. Importantly, we have shown that the measured nonlinear I-V characteristics of Au nanowires can be quantitatively modeled by impurity effects which create a tunnelling barrier at the nanostructure junction. This effect, among others, points to the vital importance for understanding contacts in nano-electronic devices, and, perhaps, to exploit it for the benefit of device operation.

Acknowledgments: We gratefully acknowledge financial support from NSERC of Canada and FCAR of Quebec. H.M. thanks Dr. N. Agraït for a useful discussion on their experimental work.

[1] N. Agraït, J. G. Rodrigo, and S. Vieira, *Phys. Rev. B* **47**, 12345 (1993).
[2] J. I. Pascual, J. Méndez, J. Gómez-Herrero, A. M. Baró, and N. García, and Vu Thien Binh, *Phys. Rev. Lett* **71**, 1852 (1993).
[3] L. Olesen, E. Lægsgaard, I. Stensgaard, F. Besenbacher, J. Schiøtz, P. Stoltze, K. W. Jacobsen, and J. K. Nørskov, *Phys. Rev. Lett* **72**, 2251 (1994).
[4] J. I. Pascual, J. Méndez, J. Gómez-Herrero, A. M. Baró, and N. García, Uzi Landman, W. D. Luedtke, E. N. Bogachek, and H. P. Cheng, *Science* **267**, 1793 (1995).
[5] M. Brandbyge, J. Schiøtz, M. R. Sørensen, P. Stoltze, K. W. Jacobsen, J. K. Nørskov, L. Olesen, E. Lægsgaard, I. Stensgaard, and F. Besenbacher, *Phys. Rev. B* **52**, 8499 (1995).
[6] N. Agraït, G. Rubio, and S. Vieira, *Phys. Rev. Lett* **74**, 3995 (1995).
[7] D. P. E. Smith, *Science* **169**, 371 (1995).
[8] Zheng Gai, Yi He, Hongbin Yu, and W. S. Yang, *Phys. Rev. B* **53**, 1042 (1996).
[9] A. Stalder and U. Dürig, *Appl. Phys. Lett.* **68**, 637 (1996).
[10] G. Rubio, N. Agraït and S. Vieira, *Phys. Rev. Lett* **76**, 2302 (1996).
[11] C. Sirvent, J. G. Rodrigo, S. Vieira, L. Jurczyszyn, N. Mingo, and F. Flores, *Phys. Rev. B* **53**, 16086 (1996).
[12] J. L. Costa-Krämer, *Phys. Rev. B* **55**, R4875 (1997).
[13] J. L. Costa-Krämer, N. Garcïa, and H. Olin, *Phys. Rev. Lett* **78**, 4990 (1997).
[14] C. Untiedt, G. Rubio, S. Vieira, and N. Agraït, *Phys. Rev. B* **56**, 2154 (1997).
[15] G. Cross, A. Schirmeisen, A. Stalder, P. Grütter,

M.Tschudy and U. Dürig, *Phys. Rev. Lett* **80**, 4685 (1998).
[16] C. Z. Li, H. Sha, and N. J. Tao, *Phys. Rev. B* **58**, 6775 (1998).
[17] W. B. Jian, C. S. Chang, W. Y. Li, and Tien T. Tsong, *Phys. Rev. B* **59**, 3168 (1999).
[18] J. M. Krans, C. J. Muller, I. K. Yanson, Th. C. M. Govaert, R. Hesper, and J. M. van Ruitenbeek, *Phys. Rev. B* **48**, 14721 (1993).
[19] J. M. Krans, J. M. van Ruitenbeek, V. V. Fisun, I. K. Yanson, and L. J. de Jongh, *Nature* (London) **375**, 767 (1995).
[20] C. Zhou C. J. Muller, M. R. Deshpande, J. W. Sleight, and M. A. Reed, *Appl. Phys. Lett.* **67**, 1160 (1995).
[21] C. J. Muller, J. M. Krans,T. N. Todorov, and M. A. Reed, *Phys. Rev. B* **53**, 1022 (1996).
[22] E. Scheer, P. Joyez, D. Esteve, C. Urbina, and M. H. Devoret, *Phys. Rev. Lett* **78**, 3535 (1997).
[23] E. Scheer, N. Agraït, J. C. Cuevas, A. Levy Yeyati, B. Ludoph, A. Martïn-Rodero, G. R. Bollinger, J. M. van Ruitenbeek, and C. Urbina, *Nature* (London) **394**, 154 (1998).
[24] A. I. Yanson, G. R. Bollinger, H. E. van den Brom, N. Agraït, and J. M. van Ruitenbeek, *Nature* (London) **395**, 783 (1998).
[25] Hiroshi Yasuda and Akira Sakai, *Phys. Rev. B* **56**, 1069 (1997).
[26] K. Hansen, E. Lægsgaard, I. Stensgaard, and F. Besenbacher, *Phys. Rev. B* **56**, 2208 (1997).
[27] E. Tekman and S. Ciraci, *Phys. Rev. B* **43**, 7145 (1991).
[28] J. A. Torres, J. I. Pascual, J. J. Sáenz, *Phys. Rev. B* **49**, 16581 (1994).
[29] J. A. Torres and J. J. Sáenz, *Phys. Rev. Lett* **77**, 2245 (1996).
[30] A. García-Martín, J. A. Torres, and J. J. Sáenz, *Phys. Rev. B* **54**, 13448 (1996).
[31] J. I. Pascual, J. A. Torres, and J. J. Sáenz, *Phys. Rev. B* **55**, R16029 (1997).
[32] J. M. van Ruitenbeek, M. H. Devoret, D. Esteve, and C. Urbina, *Phys. Rev. B* **56**, 12566 (1997).
[33] N. D. Lang, *Phys. Rev. Lett* **79**, 1357 (1997).
[34] P. García-Mochales and P. A. Serena, *Phys. Rev. Lett* **79**, 2316 (1997).
[35] Daniel Sánchez-Portal, Carlos Untiedt, José M. Soler, Juan J. Sáenz, and Nicolás Agraït, *Phys. Rev. Lett* **79**, 4198 (1997).
[36] C. C. Wang, J.-L. Mozos, G. Taraschi, Jiang Wang and Hong Guo, *Appl. Phys. Lett.* **71**, 419 (1997).
[37] J. C. Cuevas, A. Levy Yeyati, and A. Martín-Rodero, *Phys. Rev. Lett* **80**, 1066 (1998).
[38] E. Bascones, G. Gómez-Santos, and J. J. Sáenz, *Phys. Rev. B* **57**, 2541 (1998).
[39] A. García-Martín, M. del Valle, J. J. Sáenz, J. L. Costa-Krämer and P. A. Serena, *Phys. Rev. B* **62**, 11139 (2000).
[40] T. N. Todorov and A. P. Sutton, *Phys. Rev. Lett* **70**, 2138 (1993).
[41] A. M. Bratkovsky, A. P. Sutton, and T. N. Todorov, *Phys. Rev. B* **52**, 5036 (1995).
[42] T. N. Todorov and A. P. Sutton, **PRB 54**, R14234 (1996);
[43] R. N. Barnett and Uzi Landman, *Nature* (London) **387**, 788 (1997).
[44] Mads Brandbyge, Karsten W. Jacobsen, and Jens K. Nørskov, *Phys. Rev. B* **55**, 2637 (1997);
[45] A. Levy Yeyati, A. Martín-Rodero, and F. Flores, *Phys. Rev. B* **56**, 10369 (1997).
[46] H. Mehrez and S. Ciraci, *Phys. Rev. B* **56**, 12632 (1997).
[47] H. Mehrez, S. Ciraci, C. Y. Fong and Ş. Erkoç, *J. of Phys.: Condensed Matter* **9**, 10843 (1997).
[48] Mads Brandbyge, Mads R. Sørensen and Karstn W. Jacobsen, *Phys. Rev. B* **56**, 14956 (1997).
[49] Mads R. Sørensen, Mads Brandbyge, and Karsten W. Jacobsen, *Phys. Rev. B* **57**, 3283 (1998).
[50] Hideaki Ohnishi, Yukihito Kondo and Kunio Takayanagi, *Nature* (London) **395**, 780, (1998).
[51] Masakuni Okamoto and Kunio Takayanagi, *Phys. Rev. B* **60**, 7808 (1999).
[52] Hyoung Joon Choi and Jisoon Ihm, *Phys. Rev. B* **59**, 2267 (1999).
[53] J. L.Costa-Krämer,N. García, P. García-Mochales, P. A. Serena, M. I. Marqués and A.Correia, *Phys. Rev. B* **55**, 5416 (1997).
[54] J. L. Costa-Krämer,N. García, M. Jonson, I. V. Krive, H. Olin, P.A. Serna and R. I.Shekhter, Coulomb Blockade effect,Nanoscale Science and Technology, **Vol. 348**, *NATO Advanced Study Institute Series E: Applied Sciences*, Edited by N. García, M.Nieto-Vesperinas and H. Rohree (Kluwer Academic, Dordrecht, 1998), p.1.
[55] Katsuhiro Itakura, Kenji Yuki, Shu Kurokawa, Hiroshi Yasuda and Akira Sakai, *Phys. Rev. B* **60**, 11163 (1999).
[56] K. Hansen, S. K. Nielsen, M. Brandbyge, E. Lægsgaard and F. Besenbacher, *Appl. Phys. Lett.* **77**, 708 (2000).
[57] Jeremy Taylor, Hong Guo, and Jian Wang, *Phys. Rev. B* **63**, R121104 (2001);
[58] Jeremy Taylor, Hong Guo, and Jian Wang, *Phys. Rev. B* **63**, 245407 (2001).
[59] Alex Wlasenko and Peter Grütter *(To be published).*
[60] John A. Rice, *Mathematical Statistics and Data Analysis*, Duxbury Press (Belmont, California) (1995).
[61] H. Manoharan, C. Lutz, D. Eigler *(Unpublished).*
[62] K. Hansen, S. K. Nielsen, E. Lægsgaard, I. Stensgaard and F. Besenbacher, *Review of Sc. Ins.* **71**, 1793 (2000).
[63] P. Ordejón, E. Artacho, and J. M. Soler, *Phys. Rev. B* **53**, 10441 (1996).
[64] G. B. Bachelet, D. R. Hamann and M. Schlüter, *Phys. Rev. B* **26**, 4199 (1982).
[65] M. Büttiker, *IBM J. Res. Dev.* **32**, 317 (1988).
[66] Brian Larade, Jeremy Taylor, H. Mehrez, and Hong Guo, *to be published in Phys. Rev. B* .
[67] N. Agraït (private communication); In an STM set up performed in UHV, initially non-linear I-V characteristics are seen; but if the tip is retracted and indented into the sample for few times, I-V characteristics becomes linear. This is clear indication of wearing out the impurity from the junction.
[68] Mads Brandbyge, Nobuhiko Kobayashi and Masura Tsukada, *Phys. Rev. B* **60**, 17064, (1999).
[69] Dmitrii L. Maslov and Michael Stone, *Phys. Rev. B* **52**, R5539 (1992).
[70] S. Datta, *Electronic Transport in Mesescopic Systems*, Cambridge University Press, New York, (1995).
[71] Dongxiao Yue, L. I. Glazman and K. A. Matreev, *Phys.*

Rev. B **49**, 1966 (1994).

FIG. 1. (a)-Schematic of the experimental set-up with a mechanical controllable break junction (MCBJ) shown at the centre with Au wires attached. (b)-DC conductance I/V (lower) and differential conductance $\delta I/\delta V$ (upper) plotted vs V; Inset is the I-V curve. The dashed line, with slope $\simeq 2.2G_0$, corresponds to linear behavior and helps to recognize nonlinearity. These experimental results are measured over a 5 *second* voltage sweep from positive (dark) to negative (grey) bias.

FIG. 2. (a)-The Shape function (S,Eq.2) vs V calculated from the data shown in Fig.1-b. (b)-Normalized functional form of the voltage $f_0(V)$ with linear dashed line shown to help view the onset of non linearity. (c)- Unbiased Conductance $g(X)$ vs V. (d)-Normalised conductance, $\delta f/\delta V$ vs V; with the inset corresponding to a magnified section of the same data to show more clearly fine details. In all graphs, dark (grey) lines correspond to positive (negative) bias.

FIG. 3. I-V characteristics of Au contacts with Hollow site registry (A) and Top site registry (B); with zero-bias conductance $0.94G_0$, $0.8G_0$ for (A) and (B), respectively. The structure of the device is illustrated in (a) where LL, D and RL correspond to Left Lead, effective Device and Right Lead, respectively. The Hollow site is shown in (c) and Top site (d) where chain atoms are illustrated by dark circles. Inset (e) shows the band structure of the lead along the transport direction, the conducting band is shown by solid line. Inset (b) shows differential conductance fluctuations of the Hollow site as a grey dotted line, dark dotted line and dark continuous line for $T = 0K$, $T = 300K$ and for $T = 300K$ with 4 mV_{rms} modulation voltage taken into account; respectively.

FIG. 4. Contour plots of surface charge density at particular bias voltage $V_b(V)$ and Energy $E(eV)$ indicated on each figure. We use the same scale for all graphs to compare the conductance probability for each configuration. Dark circles correspond to atom positions along the constriction for guidance.

FIG. 5. I-V characteristics of Au contact doped with S impurity (Solid line). The dashed line has a slope $\simeq 0.67G_0$ and is shown to help view the onset of non linearity; Circles correspond to the experimental results obtained from $f_0(V)$ (Fig.2-b) and multiplied by the zero bias conductance, $0.67G_0$. The inset (a), shows the atoms registry, where dark circles show the atomic chain, grey ones are Au atoms in the leads' surface and light grey is the S atom.

FIG. 6. I-V characteristics of Au contacts with 2 S impurity (A), disordered interface (B) and disordered interface with 1 S impurity (C). The insets illustrate the corresponding structures, with S represented as a dark circle; Au atoms in the lead and the chain are shown with grey and light grey circles, respectively. (A), (B) and (C) have zero-bias conductance of $0.55G_0$, $0.915G_0$ and $0.833G_0$, respectively.

FIG. 7. Scaled transmission coefficient $T(E)$ at $V_b = 0$ (dashed line) and $V_b = 0.136V$ (solid line) for ideal contact structure at the top site (a), 1 S impurity structure (b), disordered interface (c) and disordered interface with 1 S impurity (d). The scaling factor is $T(E = 0, V_b = 0)$.

FIG. 8. (a) Average Hartree potential (V_H) across the central cross section ($\sim 9\mathring{A}^2$) of the ideal contact at the top site; dotted line at zero bias, and dashed line at $V_b = 0.5V$; and (b) their difference showing that most of the potential drops symmetrically at the interfaces. Black circles correspond to atom positions along the constriction for guidance

FIG. 9. Conductance calculated from renormalized transmission due to backscattering as a function of bias voltage; (a) for $T_0 = 0.99, 0.9, 0.8$ corresponding to solid, dashed and dotted line, respectively with interaction parameter $\alpha = 1.0$ and (b) for $T_0 = 0.9$ and interaction parameter $\alpha = 0.1, 0.5, 1.0$ corresponding to solid, dashed and dotted line, respectively.

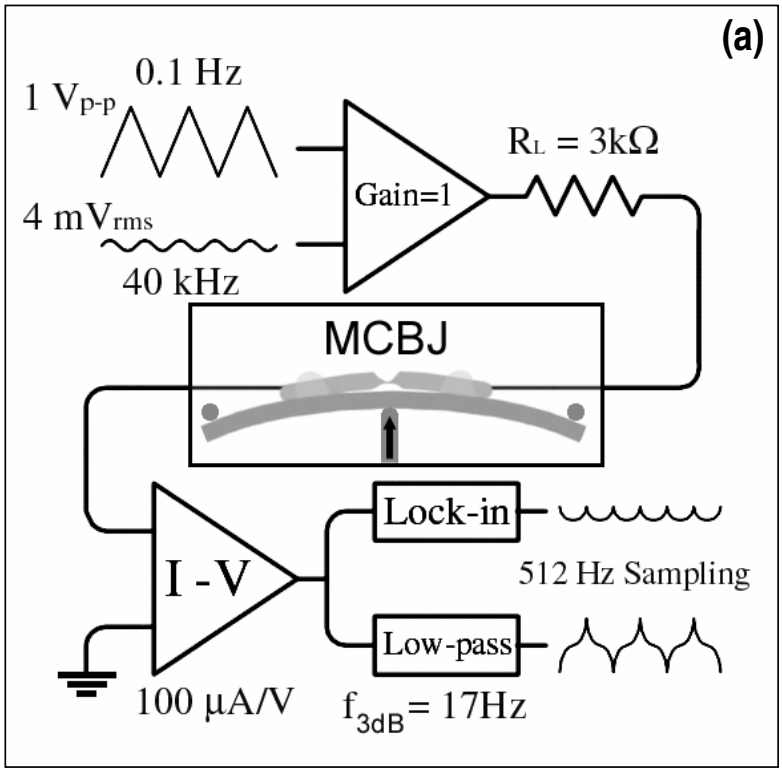
(a)
1 Vp-p
0.1 Hz
4 mVrms
40 kHz
Gain=1
RL = 3kΩ
MCBJ
Lock-in
512 Hz Sampling
I -V
Low-pass
100 µA/V
f3dB= 17Hz

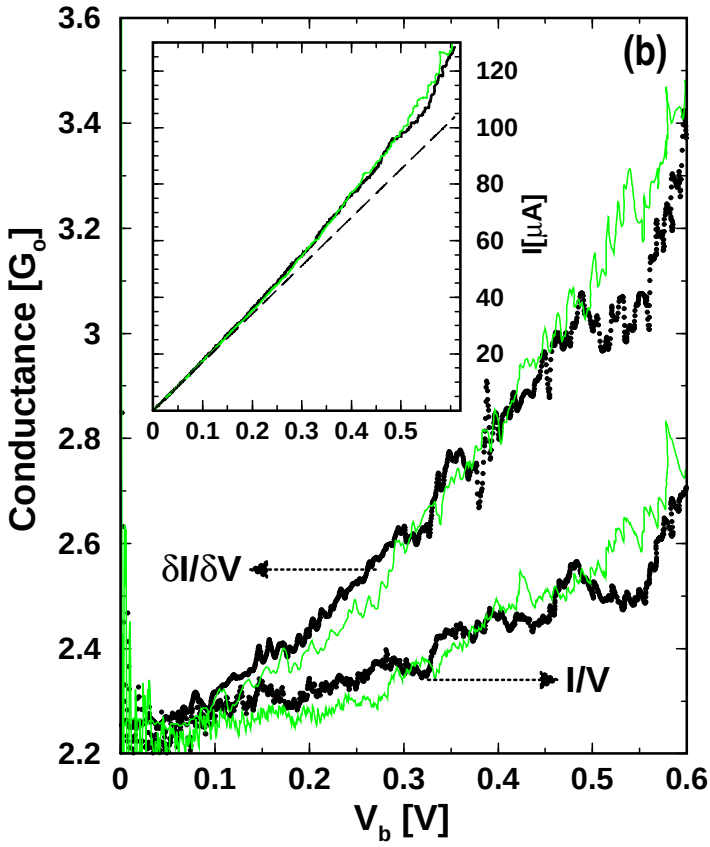
(b)
Conductance [Go]
Vb [V]
I[µA]
δI/δV
I/V
3.6
3.4
3.2
3
2.8
2.6
2.4
2.2
0
0.1
0.2
0.3
0.4
0.5
0.6
120
100
80
60
40
20

Fig.1

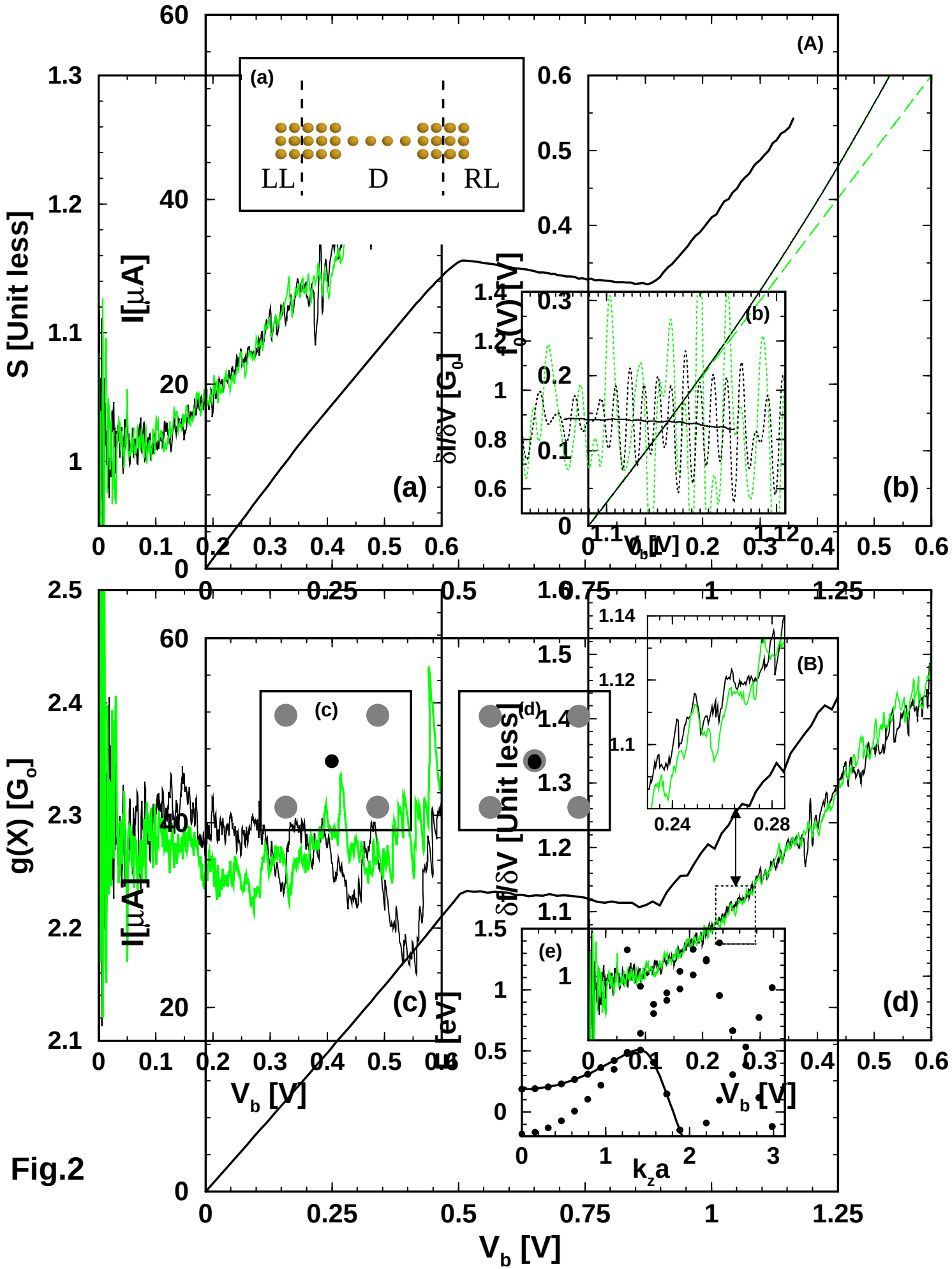
(A)
(a)
LL
D
RL
S [Unit less]
I[μA]
δI/δV [G0]
T(V)
(b)
(a)
(b)
Vb [V]
g(X) [G0]
(c)
(d)
(B)
(e)
δI/δV [Unit less]
E [eV]
kza
(c)
(d)
Vb [V]
Vb [V]

Fig.2

Fig.3

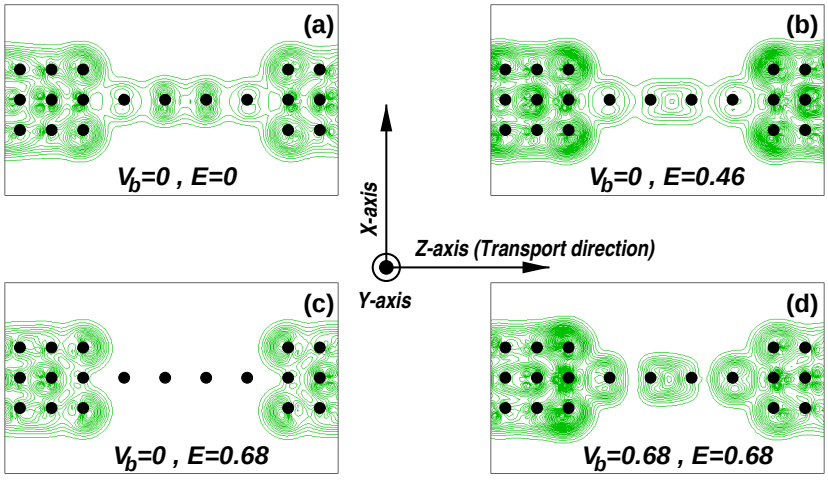
(a)
V_b=0 , E=0
(b)
V_b=0 , E=0.46
X-axis
Z-axis (Transport direction)
Y-axis
(c)
V_b=0 , E=0.68
(d)
V_b=0.68 , E=0.68

Fig.4

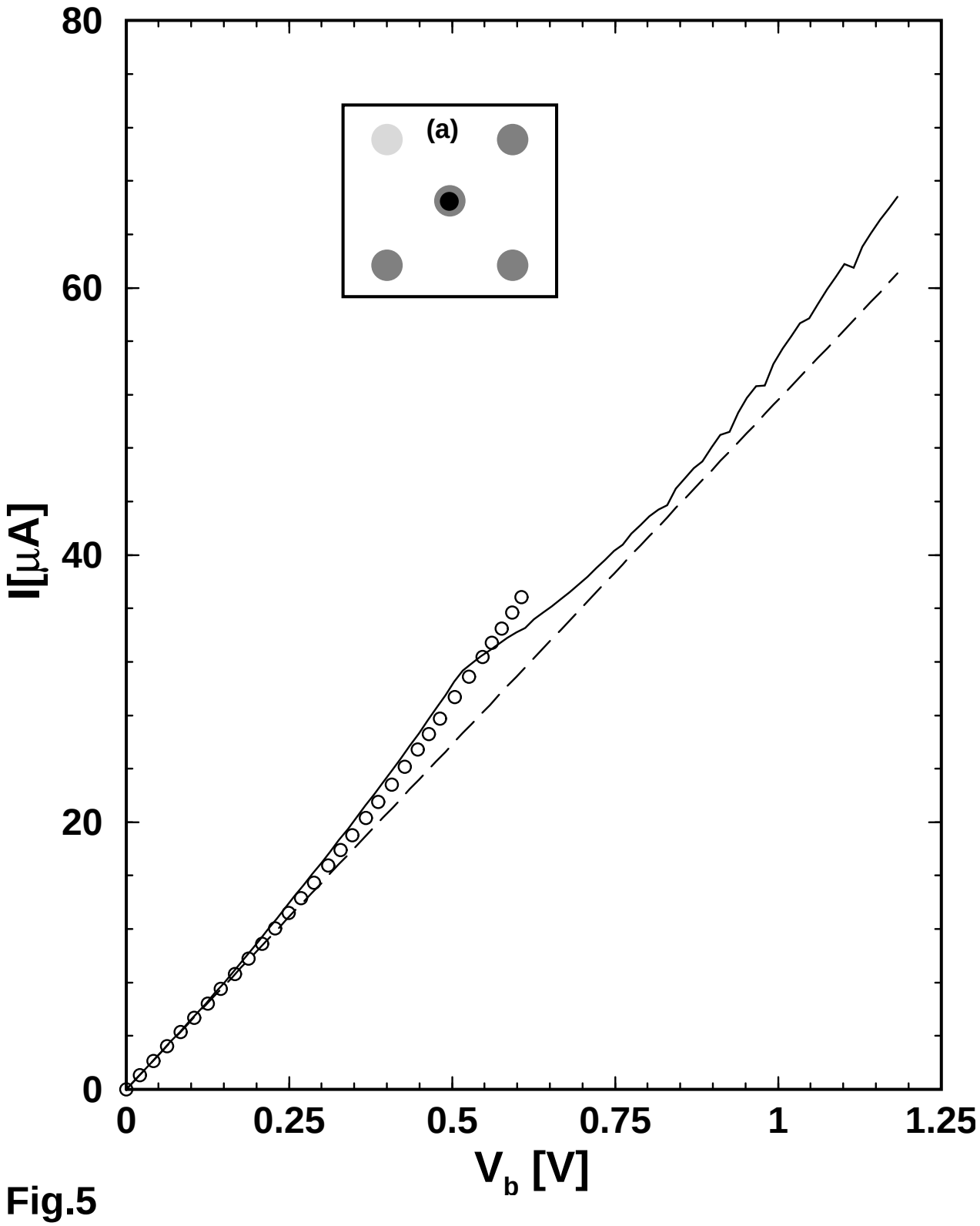

Fig.5

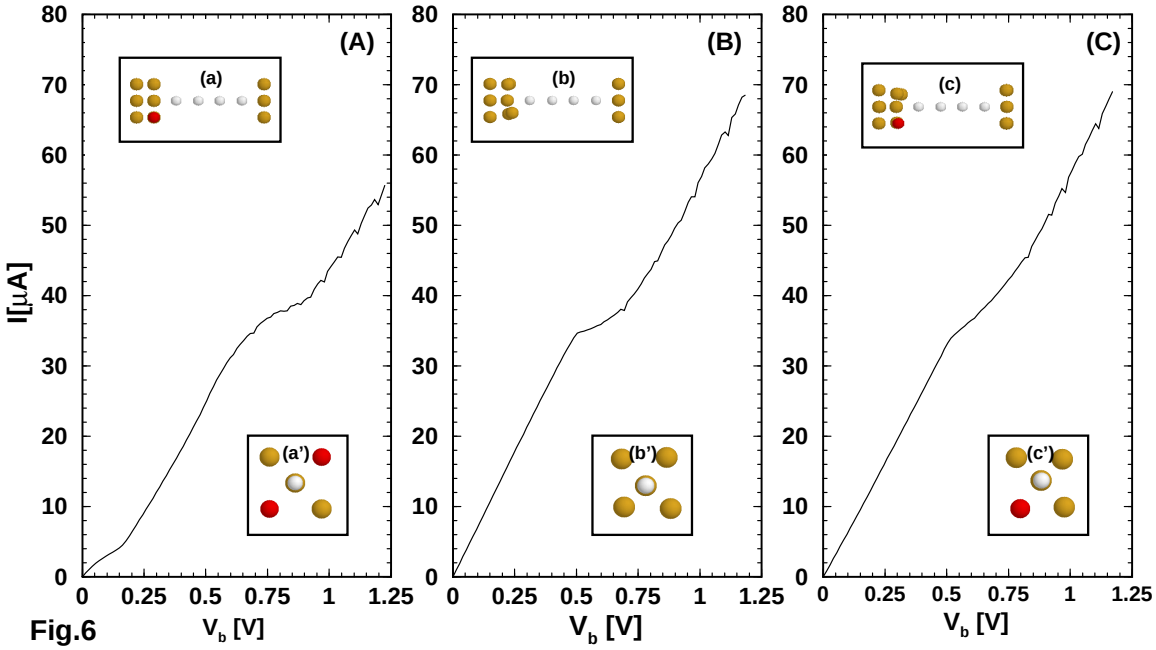

Fig.6

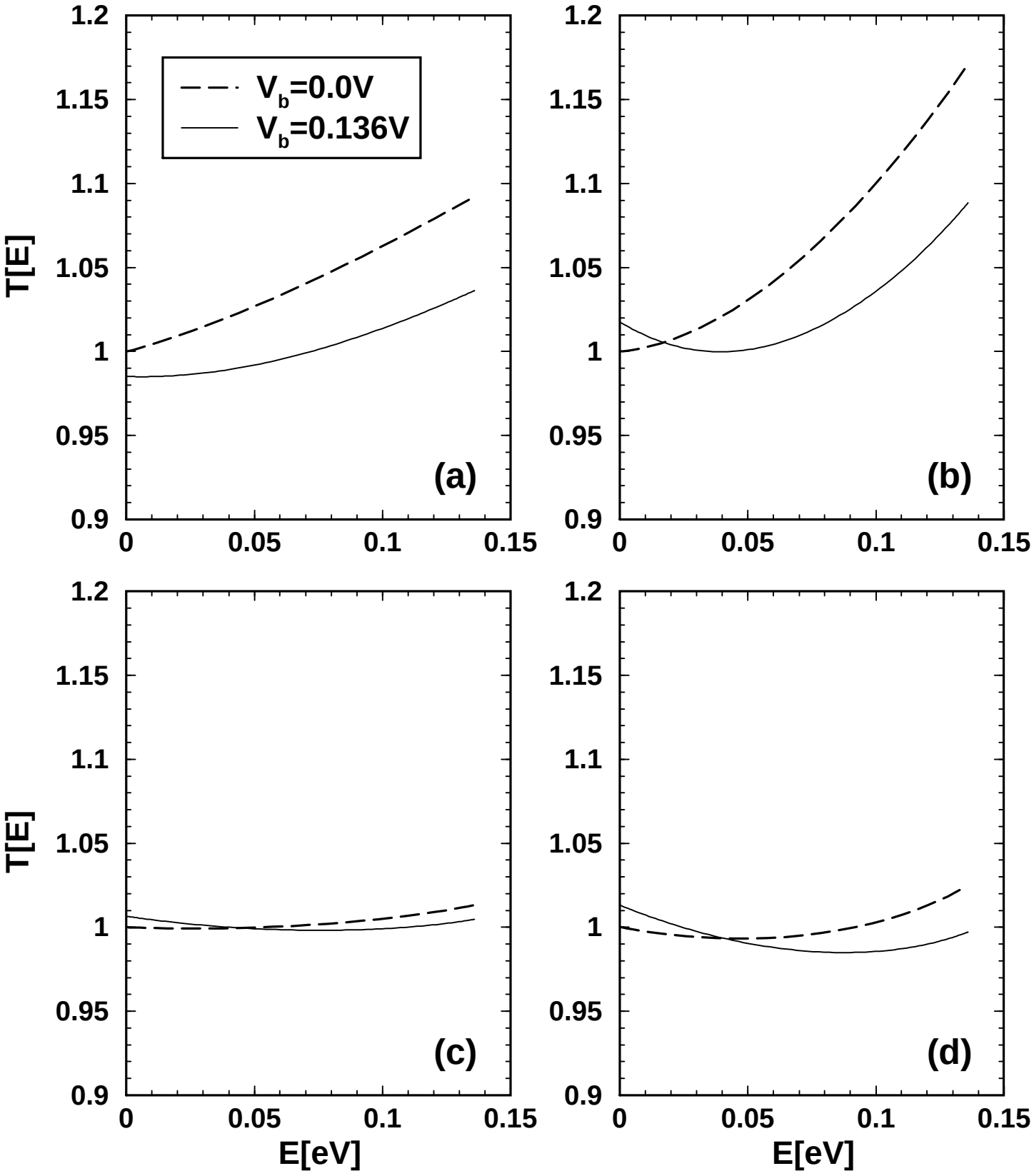

Fig.7

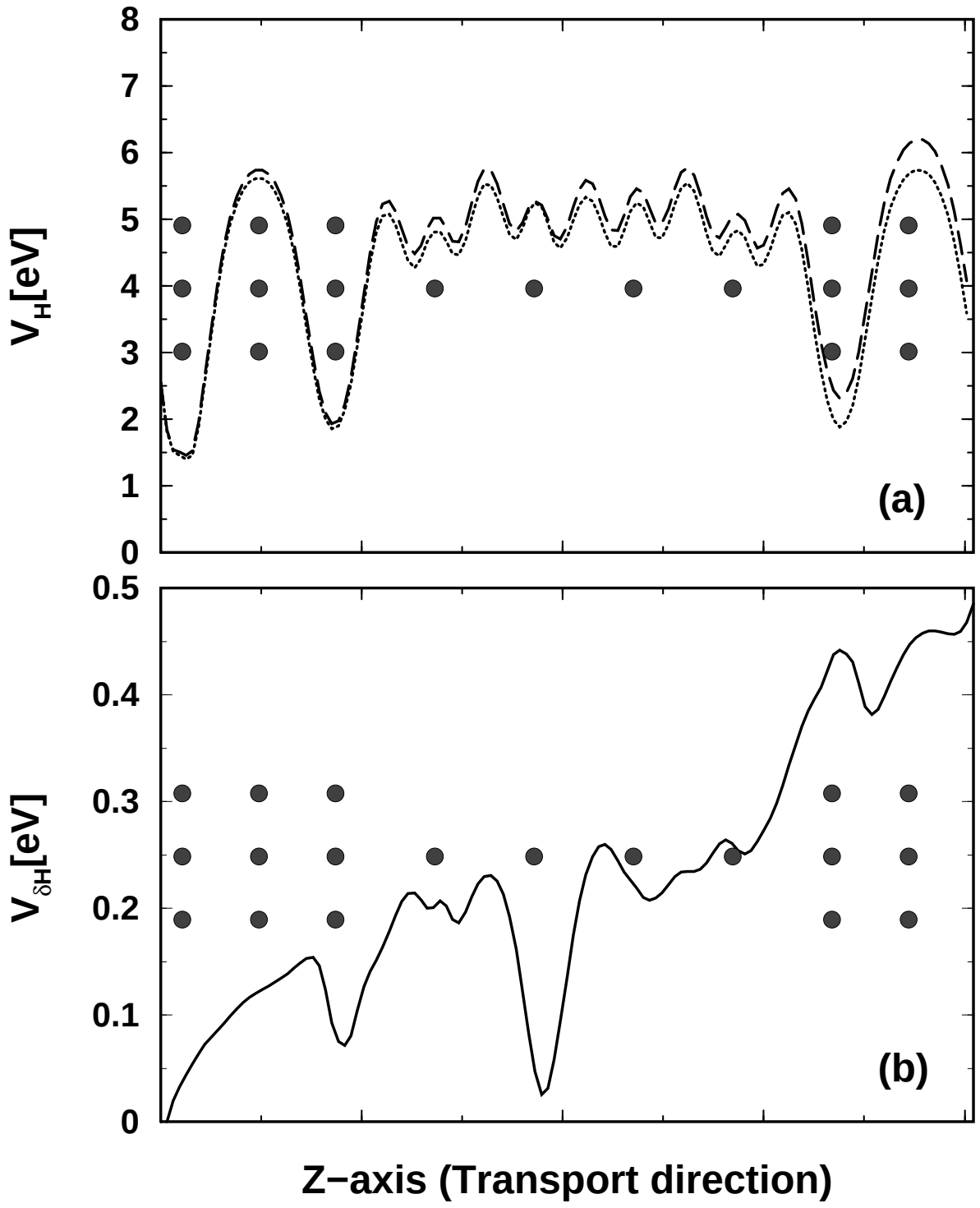
8
7
6
5
4
3
2
1
0
V_H[eV]
(a)
0.5
0.4
0.3
0.2
0.1
0
$V_{\delta H}$[eV]
(b)
Z−axis (Transport direction)

Fig.8